Available online at www.sciencedirect.com
SCIENCE DIRECT
Polymer 46 (2005) 3275–3288
polymer
www.elsevier.com/locate/polymer

Synthesis of thermoplastic polyurethane nanocomposites of reactive nanoclay by bulk polymerization methods

Asim Pattanayak, Sadhan C. Jana*

Department of Polymer Engineering, University of Akron, 250 South Forge Street, Akron, OH 44325-0301, USA

Received 14 December 2004; received in revised form 19 February 2005; accepted 23 February 2005
Available online 21 March 2005

Abstract

This paper reports synthesis and characterization of thermoplastic polyurethane nanocomposites of reactive silicate clays. Pre-polymer (method I) and chain-extended polymer molecules (method II) with residual –NCO groups participated in tethering reactions with clay during clay–polymer mixing. It was found that both clay–polymer reactions and shear stress of mixing are responsible for clay exfoliation. In method I, more clay-tethered polymer chains were produced, but clay particles did not exfoliate due to low shear stress of mixing. Method II provided an order of magnitude higher shear stress of mixing and yielded exfoliated nanocomposites. Control experiments with high shear stress of mixing and no clay–polymer reactions resulted in only intercalated composites. It was found that clay particles deterred hydrogen bonding among hard segments. The exfoliated nanocomposites exhibited optical clarity and more than 100% increase in tensile strength and tensile modulus over pristine polyurethanes.

Keywords: Bulk-polymerization; Reactive clay; Nanocomposites

1. Introduction

Polyurethanes have widespread applications as coatings, adhesives, foams, rubbers, and thermoplastic elastomers [1–3]. Often a library of raw material systems is called upon, usually by heuristics, to design specific polyurethane products. The advent of polymer nanotechnology can be capitalized under these circumstances to obtain a variety of properties from the same set of organic raw materials through introduction of nanoscopic filler particles, such as layered silicates and carbon nanotubes and nanofibers, often with the possibility of polymer chain-nanoparticle reactions. The type of nanofillers and their state and degree of dispersion can be manipulated to obtain an array of properties so far not achievable from polyurethanes or polyurethanes filled with micrometer size inorganic filler particles [4–22]. Incidentally, small quantities of nanofillers, in the range of 3–5 wt%, prove to be sufficient to bring out enormous enhancement in properties, thereby, reducing the cost and causing a drop in the weight of finished articles in comparison to conventional microcomposites of silica or talc.

The results reported to date on polymer nanocomposites, including polyurethane nanocomposites, highlight dramatic increases in tensile modulus, accompanied often by increased tensile strength and reduced elongation. Toyota researchers first demonstrated this in polyamide-clay nanocomposites—as much as 100% increase in stiffness and 50% increase in strength, for only 4 wt% nanoclay loading, were observed [23]. Wang and Pinnavaia [4] showed large enhancement in tensile strength and tensile modulus in intercalated composites of organically treated nanoclay and polyurethanes. Subsequent studies [5–22] on polyurethane–nanoclay composites reported enhancement in tensile strength, modulus, and elongation at break except for one study [5], where a decrease of tensile modulus was observed.

A first study on clay-tethered polyurethane nanocomposites was reported by Tien and Wei [10,14]; organically treated clay particles containing 1–3 $-CH_2OH$ groups per organic ammonium ion were allowed to react with pre-polymers containing –NCO end groups in solutions in *N*,*N*′dimethylformamide. The appearance of hydrogen-bonded carbonyl

* Corresponding author. Tel.: +1 330 972 8293; fax: +1 330 258 2339.
E-mail address: janas@uakron.edu (S.C. Jana).

0032-3861/$ - see front matter © 2005 Elsevier Ltd. All rights reserved.
doi:10.1016/j.polymer.2005.02.081

and –NH peaks in Fourier transform infrared spectra of reaction products of diphenylmethane diisocyanate and treated clay containing $–CH_2OH$ groups provided evidence for clay–polymer reactions. These authors observed clay layer separation by at least 4 nm and reported large enhancements in tensile and barrier properties. Osman et al. [22] prepared polyurethane adhesive nanocomposites in solution and found substantial reduction in permeability of oxygen and water vapor due to partial exfoliation of clay particles. These authors, however, did not observe evidence of clay–polymer reactions, even though the organic treatment on clay particles contained $–CH_2OH$ groups.

The use of solvents limits the scope of industrial implementation of a majority of prior work on polyurethane nanocomposites. Although solvents eliminate the diffusional limitations and provide isothermal conditions during polymer preparation, their removal from the final product becomes a serious issue. Some recent studies on bulk polymerization methods reported results similar to those using solvents, e.g. exfoliated and intercalated clay structures resulted upon clay–polymer mixing [21] and materials exhibited increases in tensile strength and elongation at break [13,17,18]. Although attractive for industrial implementation, many relevant issues in bulk polymerization need to be explored. First, diffusional limitations hinder the rates of polymerization as well as clay–polymer tethering reactions. Second, reaction conditions are seldom isothermal; increased temperature may trigger many side reactions, e.g. formation of biurets and allophanates [24,25]. Nevertheless, bulk polymerization methods offer much larger shear forces during mixing than in solution, which can potentially produce better dispersion. The present paper establishes the possibility of clay–polymer reactions in two bulk polymerization schemes by considering both reactive and non-reactive clays. For this purpose, pre-polymer and chain-extended polymer carrying residual –NCO groups were allowed to react with clay in the mixing step. Prior intercalation of clay with polyol, butanediol, or isocyanates was avoided.

2. Experimental

2.1. Materials

Thermoplastic polyurethane (PU) chains were synthesized from polyetherpolyol (Bayer ARCOL PPG 1025) with weight average molecular weight (M_w) $\sim$1020, diphenylmethane diisocyanate (MDI, Bayer Mondur *M*, $M_w = 250$ and melting point 39 °C), and 1,4-butanediol (BD, Fisher Scientific). The chain extension reactions between pre-polymer and BD was catalyzed by dibutyltinlaureate (DABCO 120, Aldrich) catalyst.

Untreated clay particle, Cloisite®NA+ (clay 1) with cation exchange capacity of 92 meq/100 g clay and treated clay particle, Cloisite®30B (clay 2) were obtained from Southern Clay Products (Gonzales, TX); the latter clay contained 90 meq of quaternary ammonium ions per 100 g clay [26]. The second specimen of organically treated clay (clay 3) was prepared in our laboratory by ion exchange of clay 1 with hexadecylammonium chloride [27]. Clay 3 contained 129 meq of hexadecylammonium ion per 100 g of clay, indicating an excess of ammonium ions adsorbed onto the clay. Among these clay particles, only clay 2 was reactive to –NCO end groups of polymer chains via $–CH_2CH_2OH$ groups in the structure of the quaternary ammonium ion, $N^+(CH_2CH_2OH)_2(CH_3)T$, where T represents an alkyl group with approximately 65% $C_{18}H_{37}$, 30% $C_{16}H_{33}$, 5% $C_{14}H_{29}$ [26].

The treated clay specimens showed particle agglomerates in the size range of 5–20 μm as revealed from scanning electron micrograph (SEM) images, although individual particles of clay were of 1 nm thickness [28]. Fig. 1 presents a representative SEM image of clay 2. These clay particles contained approximately 2 wt% moisture, which was removed by drying in vacuum oven at 80 °C for 24 h. It was noted that dried clay particles reabsorbed some moisture when taken out of the vacuum oven, e.g. clay 1 absorbed approximately 0.23 wt% moisture and clay 2 and 3 absorbed approximately 0.29 wt% moisture when kept for 5 min in a room with 50% relative humidity. To avoid significant moisture absorption, dried clay particles were hand mixed quickly with other ingredients, usually in less than 5 min, before other steps were undertaken.

Table 1 presents molar ratios of various components used in the preparation of polyurethanes with 36% hard segments. The $–CH_2CH_2OH$ groups in clay 2 were taken into consideration while balancing the ratio of –NCO and –OH groups in clay composites. The basis of such calculation was 90 meq of quaternary ammonium ion per

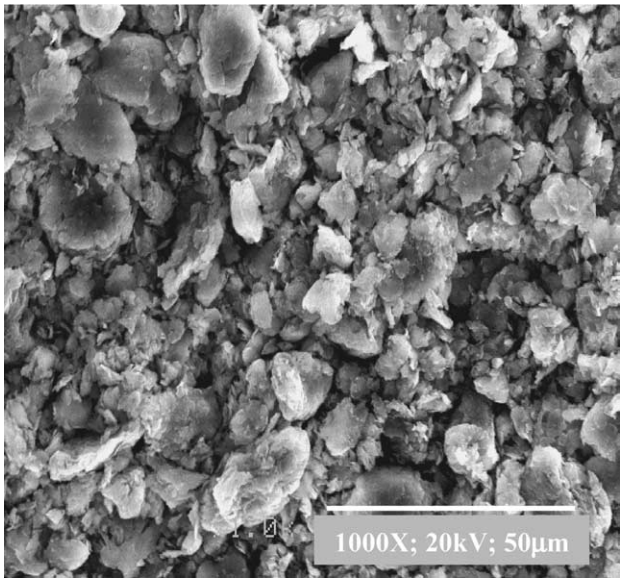

Fig. 1. Scanning electron micrographs of clay 2.

Table 1
Mole ratio of various components

Material	Clay content (wt%)	MDI/polyol/BD/clay –OH
Pristine polyurethane	0	2/1/1/0
With clay 1	1	2/1/1/0
	3	2/1/1/0
	5	2/1/1/0
With clay 3	1	2/1/1/0
	3	2/1/1/0
	5	2/1/1/0
With clay 2	1	2/1/0.98/0.02
	3	2/1/0.96/0.04
	5	2/1/0.93/0.07

100 g of clay 2. Note that trace amounts of moisture absorbed by the clay particles during sample preparation was not considered in balancing –NCO and –OH groups in Table 1. The amounts of treated clay in the composites were maintained at 1, 3, and 5 wt%, which translated to, respectively, 0.76, 2.3, and 3.8 wt% organic-free clay in the case of clay 2 and 0.74, 2.2, and 3.7 wt% organic-free clay in the case of clay 3. In the rest of the text, the clay content will be reported in weight percent of treated clay, which contained both organic treatment and organic-free clay particles.

2.2. Nanocomposites preparation

Polyetherpolyol and BD were dried overnight at 50 °C and MDI was dried at room temperature for 1 h in vacuum oven to remove the traces of moisture. Nanocomposites and pristine polyurethane were prepared by a two-step process as depicted in Fig. 2. The pre-polymer was prepared by reacting MDI with polyol for 2 h at 80 °C with stirring in a three-neck round bottom flask under nitrogen sweep. The temperature was maintained using an oil bath. The time-period of 2 h was sufficient for complete conversion of –OH groups, as found by titration of –NCO groups with dibutylamine [29]. The number (M_n) and weight average (M_w) molecular weight of pre-polymer was determined by gel permeation chromatography (GPC): $M_n \sim 2800$ and $M_w \sim 4300$.

In method I (Fig. 2(a)), clay particles were mixed with pre-polymer for 1 h at 80 °C with stirring in a three-neck round bottom flask under nitrogen sweep. The temperature was maintained at 80 °C using an oil bath. The pre-polymer-clay reaction was allowed to undergo chain extension with BD for 15 min in Brabender Plasticorder with a starting temperature of 80 °C. This reaction was catalyzed by dibutyltinlaureate at a concentration of 2.3×10^{-7} mol/cm^3. The reaction temperature increased to 120 °C in 3 min and remained stable at 120 °C for the rest of the period. Tien and Wei [10] used the same methodology to prepare nanocomposites of polyurethanes in solution.

In method II (Fig. 2(b)), chain extension reaction was carried out before the addition of clay particles. The pre-polymer was mixed with BD and 2.3×10^{-7} mol/cm^3 dibutyltinlaureate catalyst in Brabender Plasticorder and allowed to react at a starting temperature of 80 °C, although the reaction temperature increased to 130 °C in 3 min and remained there for the rest of the mixing period. Clay particles were added after 6 min of chain extension reactions and mixed further till the torque reached a plateau in approximately 9 min. Note that intercalation of clay

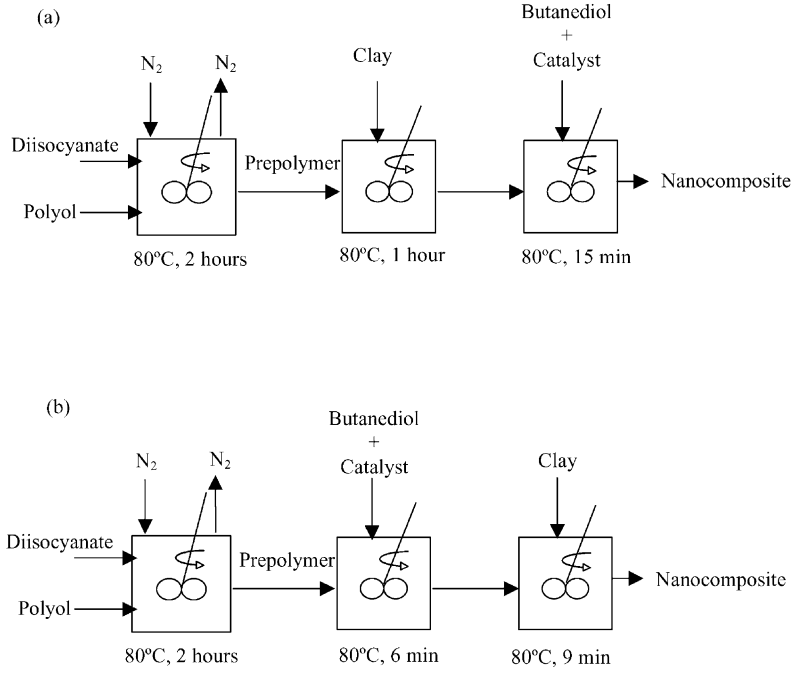

Fig. 2. Schematic of composite preparation (a) method I and (b) method II.

particles with polyol was avoided in methods I and II to allow –NCO groups to react only with the $–CH_2CH_2OH$ groups on clay particles and to produce clay-tethered polymer chains.

Chain-extended pristine polyurethane, with no residual –NCO groups, was mixed with 5 wt% clay 2 in Brabender Plasticorder for 9 min at 130 °C to prepare a material, henceforth called 'control', for comparison with that prepared by method II. In these cases, clay particle dispersion occurred under almost identical conditions of viscosity and temperature as in method II, but without the possibility of clay–polymer tethering reactions. The sample specimens for mechanical testing and characterization by X-ray were prepared by compression moulding of the composite materials at 130 °C for 5 min.

2.3. Characterization

The state of intercalation or exfoliation of nanoclay structures was investigated by wide-angle X-ray diffraction (WAXD) method and transmission electron microscopy (TEM). A Rigaku X-ray diffractometer with wavelength, $\lambda = 1.54$ Å, tube voltage of 50 kV, and tube current of 150 mA was used to obtain WAXD patterns under reflection mode: the scanning rate was 5°/min from $2\theta = 1.5$–25°. In each case, three sample specimens, cut from different parts of the materials, were tested. TEM images were obtained from approximately 50 nm thick slices using TACNAI-12 TEM device operating at 120 kV.

The clay particles and associated tethered chains were separated from the bulk polymer by extraction in a Soxhlet extraction set up using tetrahydrofuran (THF) as the solvent; the extraction was carried out for 48 h, by which time the residue reached a constant weight. Ceramic thimbles with nominal pore size of 0.2 μm were used to retain the clay particles.

The residue was subjected to reverse ion exchange reactions in a solution of lithium chloride (LiCl) in analytical grade THF [30] to release tethered polymer chains. The clay particles were separated in a centrifuge and the solution was used for molecular weight determination. The molecular weights of polymer chains were determined by Waters 510 gel permeation chromatography (GPC) system with triple detection scheme and a polystyrene standard.

The nanocomposite specimens and residue from Soxhlet extraction were characterized by Fourier-transform infrared spectroscopy (FT-IR) and differential scanning calorimetry (DSC). A Perkin Elmer FT-IR (Model 16PC) at a resolution of 4 cm^{-1} was used to obtain spectra of films of sample specimens placed between two KBr discs. The reaction between pre-polymer and clay particles was also monitored by FT-IR. A Dupont DSC (Model DSC-2910) was used under nitrogen atmosphere at scanning rate of 20 °C/min over a temperature range of −50–250 °C to determine the glass transition temperature (T_g) of polyurethane chains.

Tensile tests were performed using Instron 5567 machine, following ASTM D 638 type V method. The crosshead speed was 50 mm/min. In each case, at least five measurements were taken.

3. Results and discussion

3.1. Morphology

The state of dispersion of clay particles in materials prepared by method II was analyzed using WAXD patterns, as presented in Fig. 3. The specimens of clays 1 and 2 show broad diffraction peaks at, respectively, $2\theta = 7.4°$ (Fig. 3(a)) and $2\theta = 5.2°$ (Fig. 3(c)), while a sharp peak is observed for clay 3 in Fig. 3(b) at $2\theta = 4.8°$. On the other hand, polymer–clay composites show broad diffraction peaks at $2\theta = 3.75°$ (d-spacing ~ 2.3 nm) for clay 1, Fig. 3(a) and sharp peaks at $2\theta = 3°$ (d-spacing ~ 2.9 nm) for clay 3 in Fig. 3(b). In these cases, the presence of residual clay peaks indicates partial intercalation of clay layers by polymer chains. The weak diffraction peaks present in Fig. 3(c) at $2\theta \sim 4°$ for composites containing 1 and 3 wt% clay 2 indicate the presence of some intercalated clay structures with d-spacing

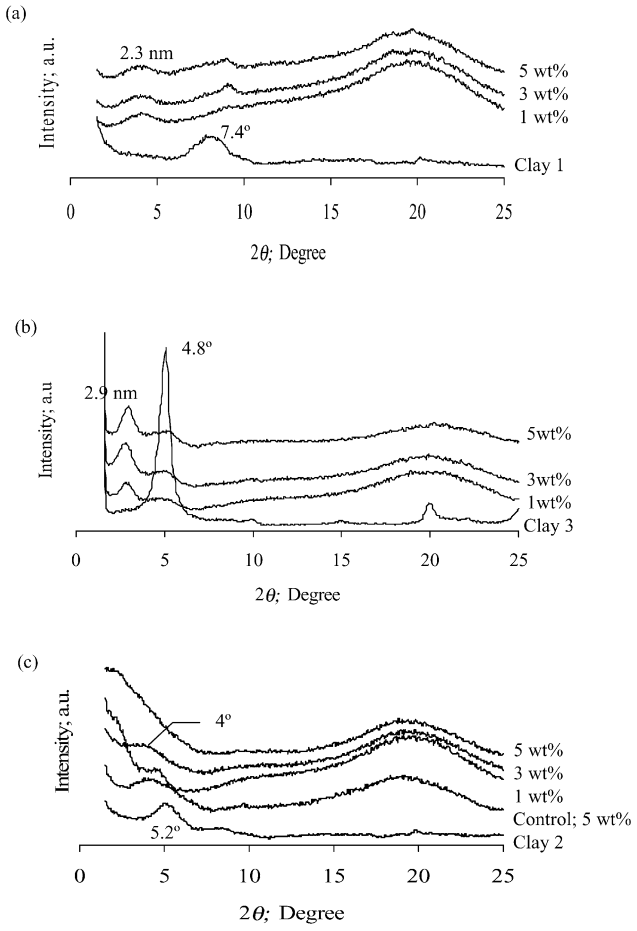

Fig. 3. WAXD patterns of nanocomposites prepared by method II of (a) clay 1 (b) clay 3, and (c) clay 2.

of 2.2 nm. However, the nanocomposite of clay 2 with 5 wt% clay shows no distinguishable peak for $2\theta > 1.5°$, although the control material with the same amount of clay 2 shows broad peak at $2\theta \sim 4°$. We resorted to transmission electron microscopy to investigate if the clay structures were exfoliated in composite materials of 5 wt% clay 2. Fig. 4 presents TEM images of composites of 5 wt% clays 1–3 prepared by method II and of composite of 5 wt% clay 2 prepared in control experiments. TEM images of other cases were not taken as the presence of original clay tactoids and partially intercalated tactoids were obvious from WAXD patterns (Fig. 3).

A large number of single platelets in Fig. 4(a) indicate that clay particles in composite of 5 wt% clay 2 prepared by method II were indeed in exfoliated state. Thus a size reduction by at least a factor of 2000 was achieved from the initial agglomerates of 5–20 μm in size (Fig. 1). In addition, many clay platelets appeared bent and, therefore, did not cause diffraction of X-rays.

TEM images of composites of 5 wt% clay 2 prepared in control experiments (Fig. 4(b)) and those of 5 wt% clay 3 (Fig. 4(c)) and clay 1 (Fig. 4(d)) prepared by method II show the presence of intercalated tactoids of thickness ranging from 200–400 nm. The apparent orientation of clay platelets in a small window of $1 \times 1\ \mu m^2$ in Fig. 4(a) seems fortuitous. Mixing in Brabender Plasticorder was not expected to produce orientation of clay particles as is clearly evident in Fig. 4(c). Recall that clay–polymer reactions were not anticipated in the mixing of clays 1 and 3, even though chain-extended polymers carried residual –NCO groups. Clay–polymer reactions were also discounted in the mixing of clay 2 and pristine polyurethane in control experiments. These results corroborate the WAXD patterns seen in Fig. 3(a)–(c)), where intercalated clay peaks were found in composites of clays 1 and 3, and control material of clay 2. The TEM images presented in Fig. 4, therefore, present evidence that efficient dispersion and exfoliation of clay particles did not occur in control materials and in materials containing non-reactive clays 1 and 3 particles.

The dispersion of clay particles was found to be poor in

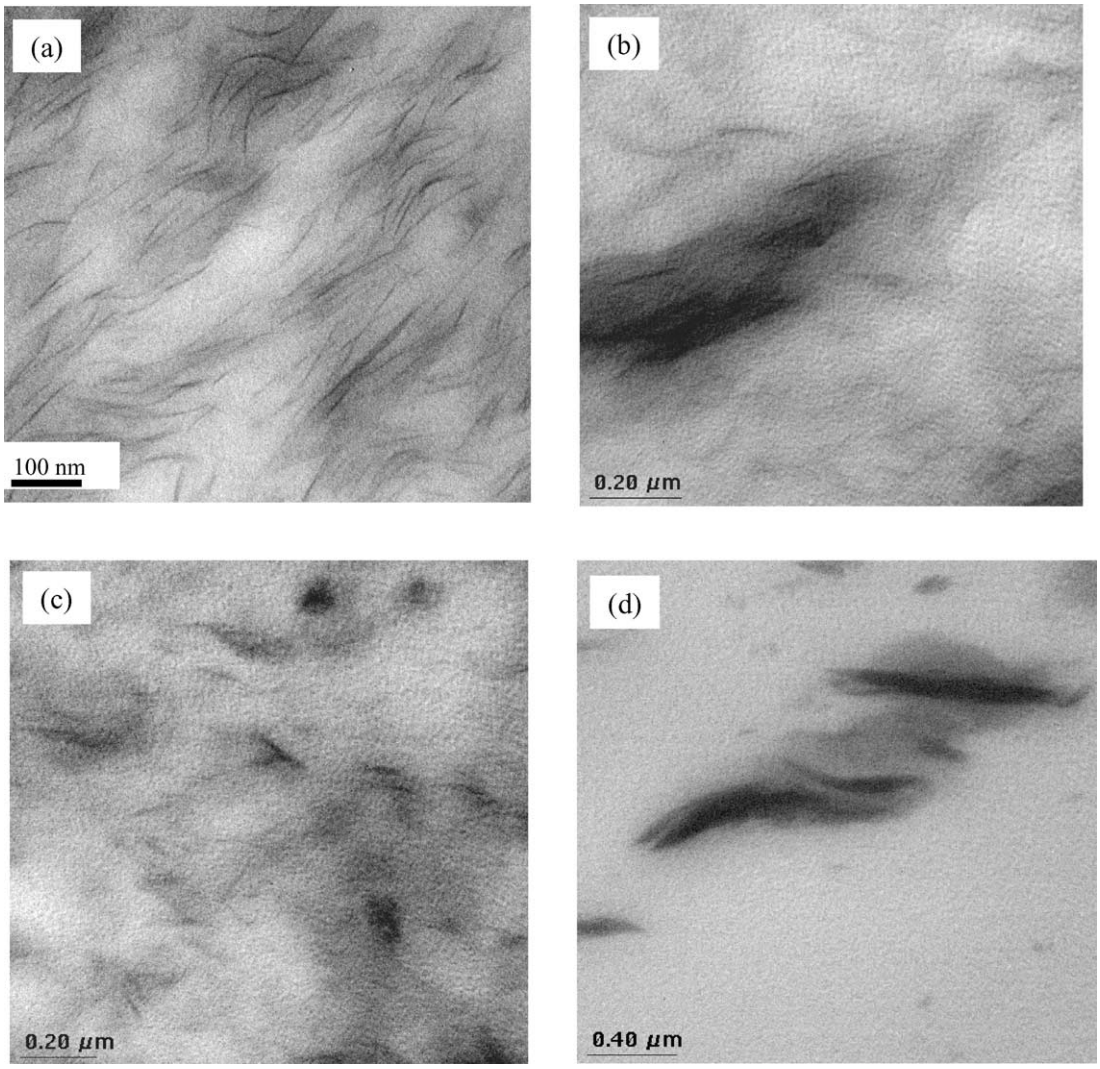

Fig. 4. TEM images of nanocomposites of 5 wt% clay (a) method II, clay 2 (b) control, clay 2 (c) method II, clay 3, and (d) method II, clay 1.

materials prepared by method I. In this case, the clay particles remained in intercalated state, irrespective of the nature of clay treatment. Representative WAXD patterns of composite of 1, 3, and 5 wt% clay 2 are presented in Fig. 5. The intercalated clay structures are also seen in the TEM image in Fig. 6—tactoids of approximately 3 μm size are present in composites of 4 wt% clay 2. In view of Figs. 5 and 6, it can be inferred that only micro-composites were produced in method I.

A ramification of excellent dispersion of clay particles in composites prepared by method II is optical clarity. Fig. 7 presents a visual demonstration of clarity of 3 mm thick sample specimens. The optical clarity of exfoliated nanocomposites of clay 2 was preserved even at clay content of 5 wt%, while that of intercalated composites of clays 1 and 3 was gradually lost with the increase of clay content.

It is apparent from Figs. 3(c) and 4(a) that dispersion of clay particles became better in method II with the increase of the amount of clay 2. Such observation is counter-intuitive and contrary to what was reported in the literature—poor dispersion is observed with the increase of clay content [10,31]. One possibility why better dispersion was achieved at higher content of clay 2 may be more clay–polymer tethering reactions, especially in the light of smaller quantities of BD used (Table 1). Before we discuss this point further, let us evaluate the extent of reactions between clay 2 and –NCO groups.

3.2. Reactivity between pre-polymer and clay

The possibility of urethane linkage formation between $–CH_2CH_2OH$ functionalities of clay 2 and –NCO end groups of polymer chains was investigated by monitoring the stretching of –NCO groups at 2270 cm^{-1} in FT-IR spectrum. For this purpose, 9 g pre-polymer and 0.5 g dried clay 2 were mixed by hand at room temperature to produce a uniform mixture. A few drops of the pre-polymer–clay mixture were kept in the chamber formed by two KBr discs and a Teflon spacer and allowed to react at 80 °C for a period of 60 min. Note that the reaction was not catalyzed and it corresponds to clay–polymer reaction in composite of 5 wt% clay 2 prepared by method I. Similar experiments were carried out to follow chemical changes in the pre-polymer and in clay–pre-polymer mixtures of clays 1 and 3.

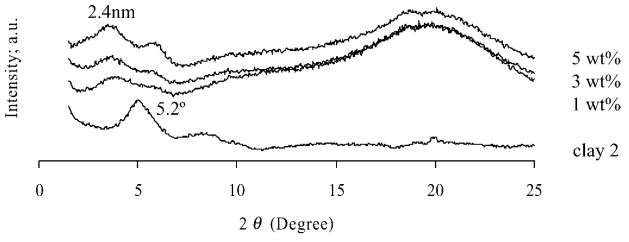

Fig. 5. WAXD patterns of nanocomposites prepared in method I with clay 2.

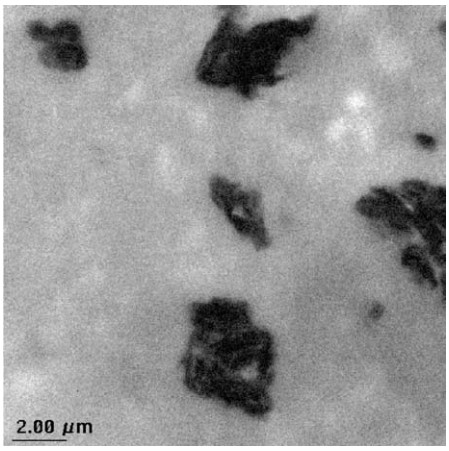

Fig. 6. TEM image of composite of clay 2 prepared by method I.

Clay–polymer reaction of method I was chosen instead of method II to exploit much higher concentration of –NCO groups in the former.

The FT-IR spectra of treated and untreated clays are presented in Fig. 8. The structural –OH stretching peak (e.g. from Al–OH bond) at 3620 cm^{-1} and hydrogen-bonded water bending peak at 1630 cm^{-1} [32] are of interest as both structural –OH and water are capable of reacting with –NCO groups. Also note that clays 2 and 3 exhibit –CH stretching peaks at 2940 and 2860 cm^{-1}, which correspond to hydrocarbon chains of the organic ammonium ions present in treated clays.

The clay–polymer reaction was followed by monitoring the stretching of –NCO and CO groups. A gradual reduction of –NCO peaks can be due to reactions with structural –OH, H_2O molecules present in clay and on KBr discs, $–CH_2CH_2OH$ groups in clay 2, or due to dimerization and trimerization reactions [24]. It is worthy to note that the organic ammonium ions, e.g. those present in treated clays, can potentially promote trimerization of –NCO groups [33]; however, this was not observed in the present study as the characteristic peaks at 1695–1715 cm^{-1} due to trimers of –NCO [24] did not appear during the course of reactions.

Note that –NCO peaks did not disappear completely in a period of 60 min. Fig. 9 shows how the conversion (α) of the –NCO group, defined as $\alpha \equiv A_{NCO,0} - A_{NCO}/A_{NCO,0}$, changed with time. Here, A_{NCO} is the area under the peak at 2270 cm^{-1} due to –NCO stretching at any time t and $A_{NCO,0}$ is the initial area of –NCO peak. A constant area under the peaks between 2860 and 2940 cm^{-1} due to –CH stretching (A_{CH}) guaranteed that the reactants did not flow out of the chamber. It is seen that $\alpha \sim 0.08$ for pre-polymer, 0.12 for pre-polymer–clay 1 mixture, and 0.09 pre-polymer–clay 3 mixture after 1 h of reaction (Fig. 9(a)). A non-zero value of α in the case of pre-polymer can be attributed to the reactions between –NCO groups and –NH groups of urethanes or between –NCO groups and trace amounts of moisture on KBr discs. Both reactions yield urea [24,25,34,35]. The formation of allophanates and biurets was ruled out

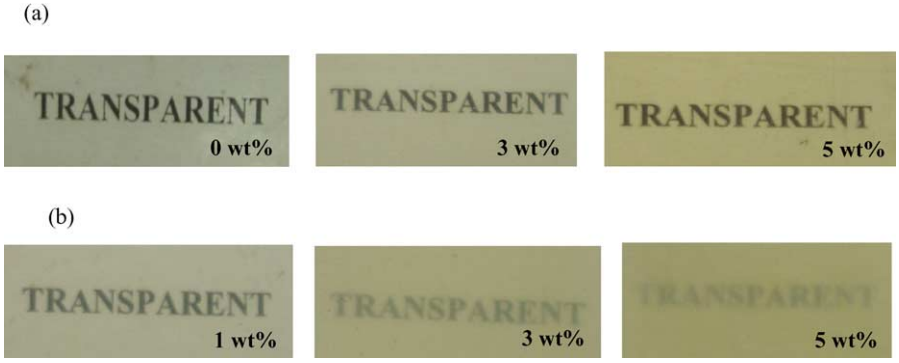

Fig. 7. Optical clarity of composites. In each case a 3 mm thick film was kept on a white paper with the word transparent written on it (a) clay 2 and (b) clay 1. Clay content is given in weight percent.

in this experiment as the reaction temperature was well below 100 °C [25]. A higher value of α in the case of clay 1 was due to additional hydrogen-bonded water present inside the clay galleries, as seen in FT-IR spectra presented in Fig. 8. In the case of clay 2, α was found to be approximately 0.38 (Fig. 9(a)). This shows that $-CH_2CH_2OH$ groups residing inside clay particles accounted for conversion of a major portion of –NCO groups. An increase in the area under the carbonyl peak (A_{CO}) at 1733 cm^{-1} indicate that the reactions between –NCO and $-CH_2CH_2OH$ groups yielded urethane linkages. This is presented in Fig. 9(b) in the form of β vs. time curves, where $\beta \equiv A_{CO} - A_{CO,0}/A_{CO,0}$ and $A_{CO,0}$ is the initial area under the CO peak. Fig. 9(b) also reveals non-zero values of β for pre-polymer and non-reactive clay particles, which can be attributed to C=O groups in urea linkages arising from the reactions between –NCO groups and moisture [25,34,35]. A large difference in the values of $\alpha \sim 0.38$ and $\beta \sim 0.23$ for clay 2 in Fig. 9 for a reaction time of 1 h indicates that not all –NCO groups were converted to urethane linkages. In this context, note that one molecule of H_2O can effectively react with two –NCO groups and form one urea carbonyl group. It is also seen from Fig. 9 that the values of α and β for clay 2 were higher than those for clays 1 and 3 at all times, endorsing that $-CH_2CH_2OH$ groups participated in clay–polymer reactions from the very beginning. In addition, comparison of the values of α and β indicate that H_2O molecules present in clay galleries caused higher consumption of –NCO groups in the cases of clays 1 and 3 than in the case of pre-polymer.

Fig. 10 presents an enlarged version of the FT-IR spectra between 3650 and 3590 cm^{-1} to show the time evolution of the peak at 3626 cm^{-1} corresponding to structural –OH

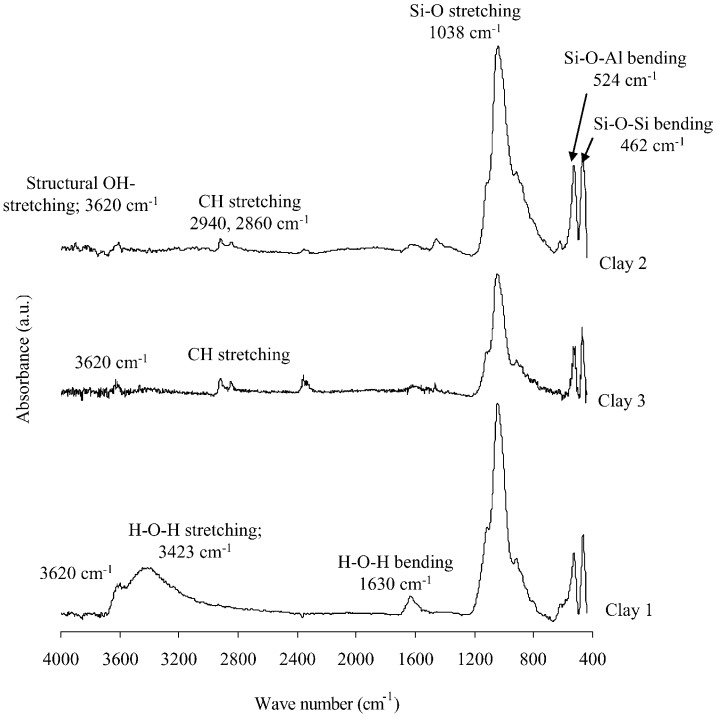

Fig. 8. FT-IR spectra of clay specimens.

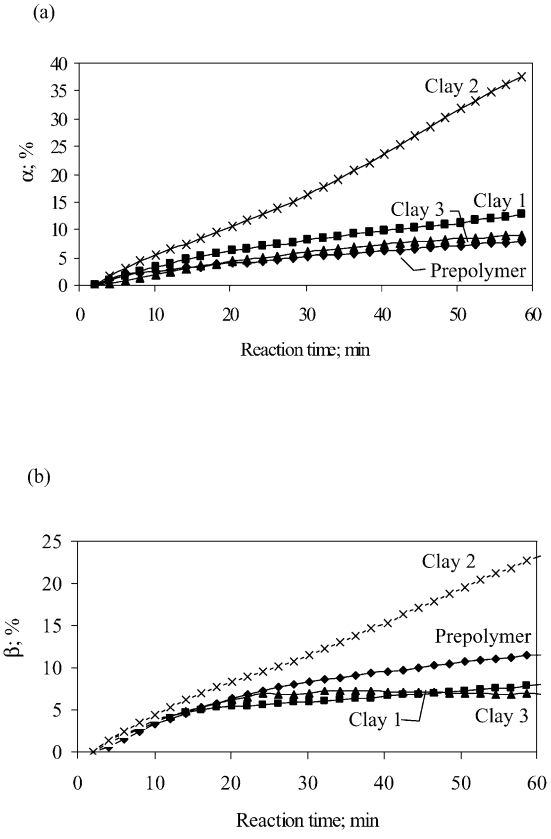

Fig. 9. Clay–pre-polymer reactions by FT-IR. (a) Percentage change of A_{NCO} and (b) A_{CO} with time.

groups. The absorbance in this band was negligibly small compared to those due to –CH and –NCO stretching. It is seen that the area under the peak at 3626 cm^{-1} decreased with time, indicating that some structural –OH groups participated in clay–polymer tethering reactions. However, the concentration of structural –OH groups in clay samples was small (Fig. 8) and the area change of the peak at 3626 cm^{-1} was insignificant compared to that of the carbonyl groups. In view of this, we note that the extent of tethering reactions directly with the structural –OH groups was much smaller compared to those with the $–CH_2CH_2OH$ groups of clay 2.

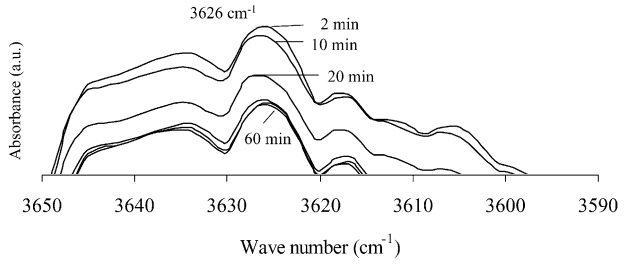

Fig. 10. FT-IR spectra showing gradual reduction of structural –OH peak at 3626 cm^{-1} during pre-polymer–clay 2 reaction at 80 °C.

3.3. Characterization of nanocomposites by FT-IR

The FT-IR spectra of chain-extended polymer and nanocomposites were analyzed to understand the effects of clay particles on hydrogen bond formation by the hard segments. Fig. 11 presents FT-IR spectra of 5 wt% clay composites prepared by method II. The FT-IR spectra of composite materials prepared by control experiment and by method I are also included, Fig. 11(f) and (g), respectively.

The clay particles in nanocomposites produced characteristic bands associated with the stretching of Si–O (1038 cm^{-1}) and Si–O–Al (524 cm^{-1}) and bending of Si–O–Si at 462 cm^{-1} [36], e.g. in Fig. 11(c)–(g). The prepolymer shows a sharp –NCO peak at 2270 cm^{-1} (Fig. 11(a)), while the absence of –NCO peaks at 2270 cm^{-1} in Fig. 11(b)–(g) indicates completion of chain extension reaction. The hydrogen-bonded NH peaks at 3290–3307 cm^{-1}, free NH peaks at 3527 cm^{-1}, and carbonyl peaks at 1701 and 1725 cm^{-1} indicate the presence of urethane linkages [37,38]. Fig. 11(b)–(g) reveals that a majority of –NH groups in urethane linkages participated in hydrogen-bonding either with the C=O group of the hard segments or with the ether linkages of the soft segments. The peaks for hydrogen-bonded NH groups shifted from 3307 cm^{-1} in pristine polyurethane to 3290 cm^{-1} in cases of composites of clays 1–3. This indicates that a majority of hydrogen-bonded NH groups in these composites was associated with the ether linkages [37,38]. The carbonyl peaks—at 1725 cm^{-1} (free) and at 1701 cm^{-1} (hydrogen-bonded)—appeared in pristine polyurethane and in composites as evident in Figs. 11 and 12. Table 2 lists the ratio of areas under various characteristic peaks and the area under the –CH peak. A significant reduction of A_{NH}/A_{CH} ratio occurred in clay composites. One may think that the hydrocarbon chains of the organic treatment of the clay contributed to CH stretching. However, the number of CH groups present in hydrocarbon chains of organically treated clay was negligibly small compared to those derived from polyol and butanediol. In addition, a reduction of the value of A_{NH}/A_{CH} ratio was also observed in composites of clay 1, which did not contain any organic treatment. In view of reduced A_{NH}/A_{CH} ratio and a shift of hydrogen-bonded –NH peaks from 3307 to 3290 cm^{-1}, one can infer that clay particles deterred hydrogen-bonding among hard segments. Let us now evaluate if the clay particles exerted similar effects on hydrogen bonding by carbonyl groups.

Fig. 12 highlights the carbonyl peaks of the composites and Table 2 lists the ratios of area under the peaks of hydrogen-bonded carbonyl groups at 1701 cm^{-1} (A_{HCO}) and free carbonyl groups at 1725 cm^{-1} (A_{CO}). The largest A_{HCO}/A_{CO} ratio is found in the case of pristine polyurethane and lowest in the case composite of clay 1, again indicating that the presence of clay particles hindered hydrogen bonding between carbonyl and NH groups of the hard segments. However, it is surprising to find that A_{HCO}/A_{CO} ratio for clay 2 composite is substantially higher than other

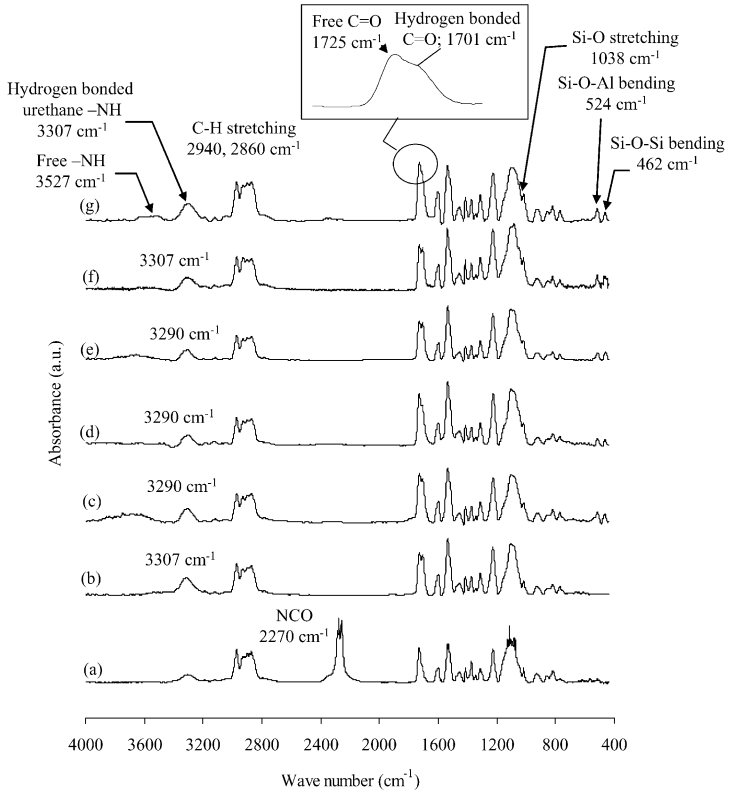

Fig. 11. FT-IR spectra of (a) pre-polymer, (b) pristine polyurethane, (c) composite of clay 1 (d) composite of clay 3, (e) composite of clay 2 all prepared by method II, (f) control compound of clay 2, and (g) composite of clay 2 prepared by method I. Clay content is 5 wt% in each case.

clay composites and is very close to that of pristine polyurethane.

The following scenarios can be constructed to explain the origin of additional hydrogen-bonded carbonyl groups in composite of clay 2. Some polymer chain ends with –NCO groups diffused to the vicinity of the clay galleries during nanocomposites preparation and reacted with $–CH_2CH_2OH$ group of the quaternary ammonium ions to produce urethane linkage, –CO–NH–. The urethane linkages, in turn, formed hydrogen bonds with the second $–CH_2CH_2OH$ group residing on the same quaternary ammonium ion, as depicted in Fig. 13. Another possibility is that C=O groups of hard segments of polyurethane chains residing in the vicinity of clay particles formed hydrogen bonds with the $–CH_2CH_2OH$ groups of the quaternary ammonium ions. The fine dispersion of clay particles seen in TEM image in Fig. 4(a) promoted such interactions. Both scenarios are supported by much lower values of A_{NH}/A_{HCO} ratio, e.g. ~2.4 in the case of clay 2, compared to ~3.2 for pristine polyurethane.

The materials prepared by control experiments of clay 2 also revealed higher values of A_{HCO}/A_{CO} ratio (0.91) than clay 1 (0.77) and clay 3 (0.78) (Table 2). However, in this case, the hydrogen-bonded –NH peak appeared at 3307 cm^{-1} (Fig. 11(f)), which indicates that most hydrogen-bonded carbonyl groups were associated with –NH

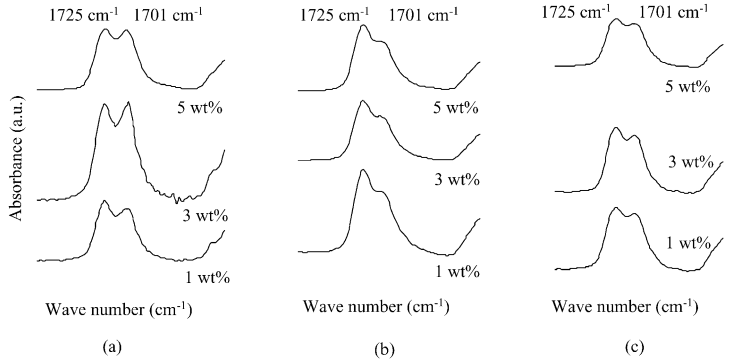

Fig. 12. FT-IR spectra of free and hydrogen bonded carbonyl peaks of composites containing 1, 3, and 5 wt% of (a) clay 2, (b) clay 3, and (c) clay 1. Composite materials were prepared by method II.

Table 2
Ratio of the area under the peak of hydrogen-bonded –NH (A_{NH}), total C=O (A_{CO}), and –CH stretching (A_{CH}) of FT-IR spectra presented in Fig. 12

Ratio	Pristine polyurethane	Composite				
		Clay 1; method II	Clay 3; method II	Clay 2; method II	Clay 2; control	Clay 2; method I
A_{NH}/A_{CH}	0.41	0.29	0.25	0.33	0.39	0.32
A_{CO}/A_{CH}	0.54	0.60	0.63	0.65	0.54	0.48
A_{HCO}/A_{FCO}	1.03	0.77	0.78	0.98	0.91	0.48

Also shown is the ratio of area under the peak of hydrogen bonded C=O (A_{HCO}) and free C=O (A_{FCO}) groups computed from Fig. 13.

groups of urethane linkages, as in pristine polyurethane (Fig. 11(b)). Consequently, hydrogen-bonding interactions between polymer chains and clay 2 particles in materials prepared by control experiments were much less than those prepared by method II, which may have led to poor dispersion of clay particles as seen in Fig. 4(b).

Two differences are readily apparent from a comparison of FT-IR spectra of composite materials prepared by method I (Fig. 11(g)) with those prepared by method II (Fig. 11(e)). First, the peak height attributed to hydrogen-bonded CO (1701 cm^{-1}) is much smaller for materials prepared by method I. Second, the ratio A_{CO}/A_{CH} is much smaller than in method II. In addition, the ratio A_{HCO}/A_{CO} is substantially smaller (0.48) than pristine polyurethane (1.04) and nanocomposite prepared by method II (0.98), see Table 2. These indicate that hydrogen bonding by urethane linkages of free polymer chains with $–CH_2CH_2OH$ groups of quaternary ammonium ions was greatly reduced in composites prepared by method I. The poor dispersion of clay particles seen in TEM image of Fig. 6 also supports this. A question comes to mind as to what fraction of the hydrogen-bonded carbonyl groups arise due to the scenario presented in Fig. 13, i.e. originated from clay-tethering reactions and subsequent hydrogen bonding. An answer to this was not apparent from FT-IR spectra. Therefore, we

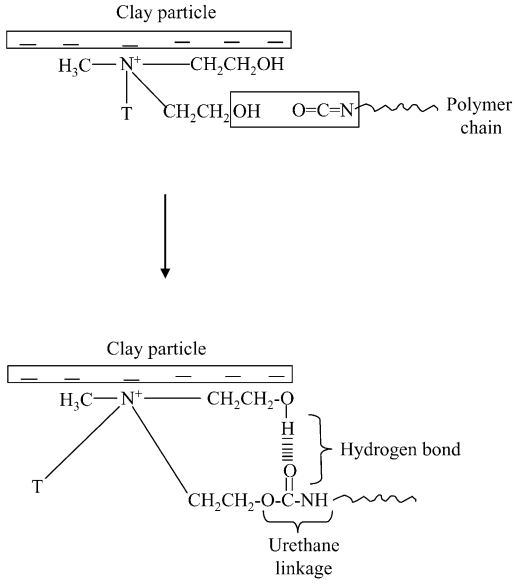

Fig. 13. Hydrogen bonding by clay-tethered polyurethane chain.

resorted to Soxhlet extraction of the composite materials to determine the amounts of residue and free, soluble polymer chains.

3.4. Clay-tethered polymer chain residues

The residue in Soxhlet thimble may reveal the amount of clay-tethered polymer chains with the exception of very small amount of polymer chains physically adsorbed on the clay particles. This is presented in Table 3 as weight percent of the original amount of the composite specimen taken for extraction.

It is apparent that methods I and II presented very different limits of the amounts of clay-tethered polymer chains. In method I, only short chain pre-polymer ($M_n \sim 2800$) was involved in clay–polymer reactions, while extended chain polymer ($M_n \sim 20{,}000$) participated in clay–polymer reactions in method II. Thus, approximately seven times greater polymer mass was tethered to clay in method II than in method I via a single clay–polymer reaction. The composition presented in Table 1 reveals that 2.36 g organic-free clay, 1.14 g quaternary ammonium ion, 20.74 g MDI, 42.33 g polyol, and 3.46 g BD were used to make 70 g composite. As the equivalent weight of the quaternary ammonium ion was 180.4 g, there were altogether 0.0063 equiv. of $–CH_2CH_2OH$ groups available for clay–polymer tethering. This can yield 0.0063 equiv. of clay-tethered polymer chains, which is approximately 18 g in method I and approximately 126 g in method II. In these calculations, a polymer chain was assumed to react only once with a quaternary ammonium ion, even though there are two $–CH_2CH_2OH$ groups per quaternary ammonium ion. A comparison of the amounts of residue obtained in Soxhlet extraction presented in Table 3 revealed that in the case of 5 wt% clay 2, only ~4 wt% of the $–CH_2CH_2OH$ groups originally present in the clay reacted in method II, while 35 wt% reacted in method I. It is accepted in the literature [28] that a substantial fraction (~20%) of the cations in montmorillonite clay is derived from the broken bonds during fracture of clay sheets and is located at the edges. In view of this, as a rough estimate, all clay-tethering reactions in method II and a majority in method I can be considered to occur with the quaternary ammonium ions located at the edges of the clay particles. Note that the residues for clays 1 and 3 were almost the same as the amounts of clay originally used. The residues were

Table 3
Residue and molecular weight of soluble polyurethane chains

Material	Clay content (wt%)	Residue (wt%)	Weight average molecular weight (M_w)	Polydispersity index (M_w/M_n)
PU	0	0	63,000	3.2
Method II; clay 1	1	0.8	75,000	2.6
	3	2.5	65,000	2.2
	5	4	61,000	2.4
Method II; clay 3	1	2	64,000	2.8
	3	4	61,000	3.0
	5	6	60,000	3.0
Method II; clay 2	1	2	85,000	4.1
	3	6	75,000	3.5
	5	8	82,000	3.7
Method I; clay 2	1	2	29,000	3
	3	7	27,000	2
	5	7	25,000	2

characterized by FT-IR and DSC to determine their chemical nature.

It is seen from FT-IR spectra in Fig. 14(a) and (b) that the residue with clay 2 has both the characteristic peaks of –C=O group at 1725 cm^{-1}, hydrogen bonded –NH at 3307 cm^{-1}, and Si–O stretching at 1038 cm^{-1}, indicating the presence of polyurethane chains and clay particles in the residue. Fig. 14(c) and (d) for non-reactive clays, however, show only the prominent Si–O stretching of the clay; a peak of very small height at 1733 cm^{-1} indicates that only a trace amount of polyurethane chains was associated with the residue, probably by physical adsorption on the clay particle surfaces. In addition, the small peaks seen at 3620 cm^{-1} due to residual structural –OH groups in Fig. 14(c) and (d) endorse our claim that clay–polymer reactions via structural –OH groups were insignificant.

3.5. Molecular weight

The molecular weights of soluble polyurethane chain extracts are presented in Table 3. In general, molecular weight of the soluble polymer from method I are much lower than in method II, e.g. $M_w = 31{,}000$ in method I vs. 85,000 in method II with 1 wt% clay 2.

It was anticipated in method II that molecular weight of clay-free polyurethane chains would not show dependence on the nature of clay particles, first due to small clay loading and second due to the fact that chain extension between butanediol and pre-polymer was carried out before clay particles were added. One possible cause for lower molecular weights in method I, especially for higher loading of clay 2, may be higher reactivity of trace amounts of moisture present in clay galleries with pre-polymer chains.

3.6. Thermal analysis

The thermal properties of composite materials are given in Table 4. The soft segments of pre-polymer and pristine polyurethane showed glass transition at, respectively, −28 and −6 °C. It is evident that glass transition temperature of soft segments of composites prepared by method II increased only slightly due to the presence of clay particles, while composites prepared by method I showed a reduction of T_g at higher clay content. The same trend is observed in

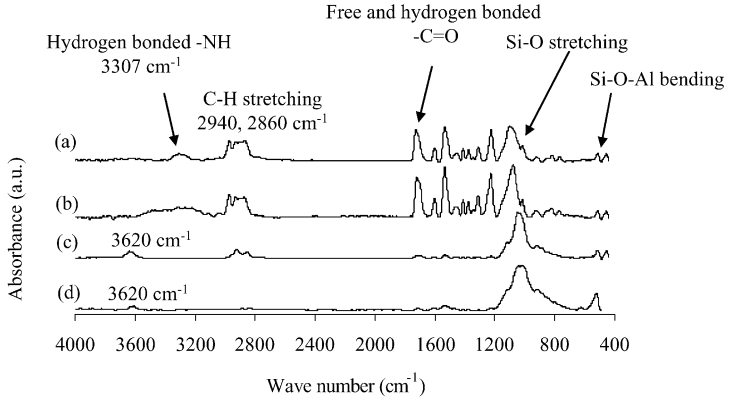

Fig. 14. FT-IR spectra of Soxhlet extracted residues of composites with 5 wt% clay. (a) Method I; clay 2 (b) method II; clay 2, (c) method II; clay 3, and (d) method II; clay 1.

Table 4
Thermal properties of polyurethane nanocomposites

Material	Clay (wt%)	T_g (°C)	T_m (°C)	T_g (°C) of residue
PU	0	−6	140	−6
Method II; clay 1	1	−3	138	−4
	3	−2	140	−4
	5	−2	146	−3
Method II; clay 3	1	−2	143	−4
	3	−2	141	−4
	5	−4	146	−4
Method II; clay 2	1	−3	141	−4
	3	−2	142	−4
	5	−1	147	−6
Method I; clay 2	1	−5	134	−12
	3	−7	133	−14
	5	−10	134	−22

residues. However, the T_g of residue from the composite of 5 wt% clay 2 prepared by method I is seen to approach the T_g of pre-polymer. This indicates that a vast majority of clay-tethered polyurethane chains in method I had molecular weights similar to pre-polymer chains. Therefore, it can be inferred that these chains did not participate in chain extension reactions with butanediol.

The values of soft segment T_g of soluble polymer chains from method II were found to be in the same neighborhood of pristine polyurethanes and were insensitive to the clay content. The soluble polymer from method I, on the other hand, showed significant reduction in the values of T_g (the same values as reported in Table 4), in line with much reduced molecular weight of soluble polymer chains as reported in Table 3.

The melting transitions, corresponding to the hard-segment phases, showed melting temperatures (T_m) of 140 °C for pristine polyurethane, 147 °C for composite of 5 wt% clay 2 prepared by method II, and 134 °C for composite of 5 wt% clay 2 prepared by method I. However, the value of enthalpy associated with melting in each case was small, indicating only very small fractions of hard segments in these materials. The residue of method I produced a T_g of −1.5 °C and that of method II a T_g of −2.5 °C. The same transition was not observed in the case of clay 1, though a small transition was noticed for clay 3 between −6 and 2 °C. These observations, along with the evidences from FT-IR, establish that a substantial amount of polyurethane chains were tethered to clay particles in the nanocomposites of clay 2 and almost none in the cases of clays 1 and 3.

3.7. Role of viscosity on clay particle dispersion

The dramatic differences in the state of dispersion of clay particles in composites prepared by methods I and II (Figs. 4 and 6) can now be examined in the light of shear viscosity of the polymer responsible for clay particle dispersion. For this purpose, the absolute values of complex viscosity (η^*) of pre-polymer and chain extended polymers were determined in APA2000 Alpha Technologies rheometer, respectively, at 80 and 130 °C with a strain of 0.14% and frequency of 10 rad/s. Recall that in method I clay particles were dispersed with pre-polymer at 80 °C. In method II, clay particles were mixed with chain-extended polymer at 130 °C. The chain extended polymers were prepared following the recipe given in Table 1 for 5 wt% clay 2. For this purpose, 1 mol of pre-polymer was mixed with 0.93 mol of butanediol and polymerized at 130 °C in the rheometer and the absolute value of η^* was noted at the end of a 10 min period. The pre-polymer was found to have a viscosity of 500 Pa s at 80 °C compared to a viscosity of 4500 Pa s at 130 °C of the chain-extended polymer. Thus the level of shear stress available in method II for particle dispersion was approximately an order of magnitude greater than in method I. Such a disparity in the level of shear stress then raises the question of whether only the shear stress was responsible for particle dispersion. Poor dispersion observed with clays 1 and 3 even in method II discounts such possibility. Poor clay dispersion was also observed in control experiments (Fig. 4(b)) even though pristine polyurethane offered slightly higher viscosity, $|\eta^*| \sim 4728$ Pa s at 130 °C compared to chain-extended polymer in method II, $|\eta^*| \sim 4500$ Pa s. In view of this, let us revisit the role of hydrogen-bonding on clay particle exfoliation in composites of clay 2 produced in method II and in control experiments. The materials prepared in control experiments showed no exfoliation of clay particles (Fig. 4(b)), although the fraction of hydrogen-bonded carbonyl group was similar to that of materials prepared in method II (Table 2). A large majority of these carbonyl groups was found to be hydrogen-bonded to –NH groups of urethane linkages, as in pristine polyurethane. In contrast, most urethane –NH groups in materials prepared by method II were hydrogen-bonded to ether linkages, which allowed carbonyl groups of urethane linkages to form hydrogen-bonding with $-CH_2CH_2OH$ groups of quaternary ammonium ions. Note that such hydrogen bonding originated posterior to exfoliation of clay 2 particles in method II—the combined effect of shear and clay–polymer

tethering reactions produced exfoliated clay particles, which in turn exposed $-CH_2CH_2OH$ groups for hydrogen bonding with carbonyl groups.

The poor dispersion of clay particles observed in method I (Figs. 5 and 6) can now be discussed. Since the level of shear stress was low, only a small quantity of clay particles underwent shear-induced delamination. Nevertheless, the concentration of –NCO groups for clay–polymer reactions was the highest in method I and the reaction was allowed for a period of 1 h at 80 °C. In addition, the values of T_g of clay-tethered polymer chain residues were seen to be in the neighborhood of pre-polymer (Table 4). Thus, it is quite likely that a large fraction of pre-polymer chains in the neighborhood of clay particles readily tethered to clay particles using both end –NCO groups, thus forming a coating of polymer layers around the clay particles and, therefore, did not participate in chain extension reactions. Note from the FT-IR study (Fig. 9(a)) that approximately 38% of the pre-polymer –NCO groups were consumed in such reactions. Consequently, the clay particles, completely coated by the tethered-polymer chains, did not undergo shearing deformation in the chain extension step and remained as agglomerates. In addition, the 0.295 wt% moisture in the clay also had a chance to react with the pre-polymer chains, thus forming urea [26,36,37] and effectively eliminating many pre-polymer chains from participation in chain extension reactions with butanediol at a later stage. A reduction in molecular weight, reported in Table 3, and a reduction in the value of A_{HCO}/A_{CO} in Table 2 support that many pre-polymer chains were tethered to clay particles by both –NCO end groups.

3.8. Tensile properties

The values of tensile strength, modulus, and elongation at break of composites are presented in Table 5. The materials prepared by method I performed poorly, as was expected in view of lower molecular weight reported in Table 3 and poor dispersion of clay particles seen in Figs. 5 and 6.

Of the materials prepared by method II, the composite of clay 2 showed higher values of modulus and tensile strength for all three clay loadings. In comparison, the composite containing 5 wt% clay 2, prepared in control experiments, showed improvement only in tensile modulus. In this case, much lower values of tensile strength and tensile elongation were obtained than those of pristine polyurethanes, which is not surprising considering micro-scale dispersion of clay particles (Fig. 4(b)) and no polymer-particle tethering. The tensile properties remained insensitive to clay content in composite of clay 1, though composite of 1 wt% clay 3 showed improvements in both stress and strain. In the case of 5 wt% clay 2, the modulus and the tensile strength reached, respectively, 3 and 12.8 MPa, which are, respectively, 110 and 160% higher than pristine polyurethane. This can be attributed both to clay-tethered polymer chains and to formation of hydrogen bonds by $-CH_2CH_2OH$ groups on nanodispersed clay particles with carbonyl groups of urethane linkages. An increase in modulus from 1.5 to 2.4 MPa is seen with the increase of content of clay 1, but the values of stress and strain at break reduced from 7.6 to 5.1 MPa and from 2850 to 2500%, respectively.

Table 5
Mechanical properties of polyurethane nanocomposites

Material	Modulus (MPa)	Maximum stress (MPa)	Strain at break (%)
Pristine polyurethane	1.4±0.1	4.7±0.04	2100
Method II; clay 1			
1 wt%	1.1±0.05	5.2±0.1	2800
3 wt%	1.3±0.06	4.9±0.2	2500
5 wt%	1.4±0.04	3.6±0.1	2000
Method II; clay 3			
1 wt%	1.5±0.1	7.2±0.7	2850
3 wt%	1.9±0.05	7.6±0.1	2700
5 wt%	2.4±0.3	5.1±0.1	2500
Method II; clay 2			
1 wt%	1.7±0.15	9.7±0.2	2500
3 wt%	2.3±0.11	11.2±0.3	2000
5 wt%	3.0±0.06	12.8±0.6	1800
Control; clay 2			
5 wt%	3.2±0.29	3.4±0.09	1100
Method I; clay 2			
1 wt%	0.5±0.05	2.6±0.03	2200
3 wt%	0.6±0.05	1.0±0.03	2300
5 wt%	0.5±0.02	0.5±0.02	4600

Average values and standard deviation are shown.

4. Conclusions

Polyurethane-clay composites of reactive and non-reactive clay particles were prepared by bulk polymerization methods. The reaction between $-CH_2CH_2OH$ functional groups on quaternary ammonium ions and –NCO groups on polymer chains was established by FT-IR. The best improvement in tensile properties was seen when the clay particles were tethered to polymer chains via clay–polymer reactions and were dispersed to the scale of individual clay layers. Of the two methods, method II yielded the best results in terms of nanoclay exfoliation and tensile properties. It was found that nanocomposites were formed only in the case of clay 2. The clay–polymer tethering reactions and large values of shear stress during clay–polymer mixing were found to be responsible for exfoliation and better dispersion of clay particles in method II. Although clay particles hindered hydrogen bond formation among hard segments, the $-CH_2CH_2OH$ groups on nanodispersed clay 2 particles formed hydrogen bonds with carbonyl groups of urethane linkages and made positive impact on tensile properties. It was seen via control experiments that high viscosity alone was not responsible in producing exfoliated clay composites—clay–polymer tethering reaction was also

needed. On the other hand, excessive polymer-clay reactions and lower viscosity in mixing step as in method I were found to be ineffective in producing nanocomposites. In addition, the lower values of T_g of residues in method I indicated that pre-polymer chains participated in clay tethering via both chain end –NCO groups and, therefore, did not participate in chain extension reactions.

Acknowledgements

Financial support was obtained from National Science Foundation in the form of CAREER Award to S. C. J. Dr Pat Sadhukhan of Bridgestone–Firestone Research is gratefully acknowledged for assisting with the TEM images.

References

[1] Woods G. The ICI polyurethanes book. New York: Wiley; 1990.
[2] Lamba NMK, Woodhouse KA, Cooper SL. Polyurethanes in biomedical applications. Boca Raton: CRC Press; 1998.
[3] Fabris HJ. Advances in urethane science and technology. New York: Technomic; 1976.
[4] Wang Z, Pinnavaia TJ. Chem Mater 1998;10:3769–71.
[5] Zilg C, Thomann R, Muelhaupt R, Finter J. Adv Mater 1999;11: 49–52.
[6] Petrovic ZS, Javni I, Waddon A, Banhegyi G. J Appl Polym Sci 2000; 76:133–51.
[7] Chen TK, Tien YI, Wei KH. Polymer 2000;41:1345–53.
[8] Xu R, Manias E, Snyder AJ, Runt J. Macromolecules 2001;34:337–9.
[9] Ma J, Zhang S, Qi Z. J Appl Polym Sci 2001;82:1444–8.
[10] Tien YI, Wei KH. Macromolecules 2001;34:9045–52.
[11] Tien YI, Wei KH. Polymer 2001;42:3213–21.
[12] Hu Y, Song L, Xu J, Yang L, Chen Z, Fan W. Colloid Polym Sci 2001; 279:819–22.
[13] Yao KJ, Song M, Hourston DJ, Luo DZ. Polymer 2002;43:1017–20.
[14] Tien YI, Wei KH. J Appl Polym Sci 2002;86:1741–8.
[15] Chang JH, An YU. J Polym Sci: Part B Polym Phys 2002;40:670–7.
[16] Tortora M, Gorrasi G, Vittoria V, Galli G, Ritrovati S, Chiellini E. Polymer 2002;43:6147–57.
[17] Zhang X, Xu R, Wu Z, Zhou C. Polym Int 2003;52:790–4.
[18] Song M, Hourston DJ, Yao KJ, Tay JKH, Ansarifar MA. J Appl Polym Sci 2003;90:3239–43.
[19] Mishra JK, Kim I, Ha CS. Macromol Rapid Commun 2003;24:671–5.
[20] Chen X, Wu L, Zhou S, You B. Polym Int 2003;52:993–8.
[21] Rhoney I, Brown S, Hudson NE, Pethrik RA. J Appl Polym Sci 2003; 91:1335–43.
[22] Osman MA, Mittal V, Morbidelli M, Suter UW. Macromolecules 2003;36:9851–8.
[23] Kojima Y, Usuki A, Kawasumi M, Okada A, Fukushima Y, Kurauchi T, et al. J Mater Res 1993;8:1185–9.
[24] Lyman DJ. Rev Macromol Chem 1966;1:191–237.
[25] Heintz AM, Duffy DJ, Hsu SL, Suen W, Chu W, Paul CW. Macromolecules 2003;36:2695–704.
[26] http://www.nanoclay.com/data/30B.htm
[27] Park JH, Jana SC. Macromolecules 2003;36:2758–68.
[28] Grim RH. Clay mineralogy. New York: Mc-Graw Hill; 1953.
[29] Jung CD. PhD Thesis, University of Akron, Akron; 2004.
[30] Messersmith PB, Giannelis EP. J Polym Sci: PartA Polym Chem 1995;33:1047–57.
[31] Park JH, Jana SC. Polymer 2003;44:2091–100.
[32] Madejova J. Vib Spectrosc 2003;31:1–10.
[33] Lin IS, Kresta JE, Frisch KC. Reaction injection molding and fast polymerization reactions, polymer science and technology. vol. 18. New York: Plenum Press; 1982. p. 147–163.
[34] Heiss HL, Combs FP, Gemeinhardt PG, Saunders JH, Hardy EE. J Ind Eng Chem 1959;51:929–34.
[35] Lu QW, Hoye TR, Macosko CW. J Polym Sci: Part A Polym Chem 2002;40:2310–28.
[36] Adler H, Bray EE, Stevens NP, Hunt JM, Keller WD, Pickett EE, Kerr PF. Infrared spectra of reference clay minerals, Report 8, American Petroleum Institute Project 49. New York: Columbia University; 1950.
[37] Lee HS, Wang YK, Macknight WJ, Hsu SL. Macromolecules 1988; 21:270–3.
[38] Coleman MM, Lee KH, Skrovanek DJ, Painter PC. Macromolecules 1986;19:2149–57.